

Field Test of Detection and Characterisation of Subsurface Ice using Broadband Spectral-Induced Polarisation

Robert E. Grimm* and David E. Stillman

Planetary Science Directorate, Southwest Research Institute, Boulder, Colorado, USA

ABSTRACT

Low-frequency (LF, $\ll 1$ kHz) electrical resistivity is useful in discriminating frozen from unfrozen ground in periglacial environments, but it cannot distinguish whether frozen materials are dry or ice-rich, nor can it provide reliable estimates of ice content. However, polarisabilities due to unfrozen, interfacial water and protonic defects in ice both have strong dielectric relaxations (frequency dependence), resulting in a large decrease in resistivity at high frequencies (HF, $\gg 1$ kHz). From laboratory measurements of samples collected at the US Army Permafrost Tunnel (Fox, Alaska), we find temperature-dependent relationships between ice volume fraction and the resistivity frequency effect (RFE, defined as the LF-normalised difference in LF and HF resistivities). We report the first field detection of H₂O polarisability in permafrost, using a broadband spectral-induced polarisation system at the permafrost tunnel. By comparing laboratory and field spectra, we found a best-fitting ice temperature of -3 ± 0.5 °C. Laboratory RFE at the selected temperature was then used to map the RFE in the tunnel wall to 45–95 per cent ice by volume. Both of these results agreed quantitatively with the bulk properties of the tunnel, and the ice content image correlated qualitatively with major permafrost features. The RFE approach may be expedient using simpler instrumentation, but the close agreement of laboratory and field spectra indicates that the ice and interfacial water signatures can be individually quantified by broadband fitting of both amplitude and phase. This will provide more accurate constitutive relations, but more importantly will yield better remote temperature measurement of the subsurface using known dependencies of the dielectric relaxation frequencies. Copyright © 2015 John Wiley & Sons, Ltd.

KEY WORDS: spectral-induced polarisation; electrical properties; frozen soil

INTRODUCTION

Measurement of the ice content in permafrost is important to understanding the evolution of periglacial landforms (e.g. French, 2007), the ecology of permafrost regions (Jorgenson and Osterkamp, 2005), the impact of permafrost thawing on the global carbon inventory (Schuur *et al.*, 2008) and the risk to infrastructure due to frost heave and thaw subsidence (e.g. Heginbottom *et al.*, 2012). Classical indicators of air temperature, surficial geology and aerial or satellite mapping give only large-scale classification, whereas coring and excavation are highly localised. Geophysical methods have the potential to fill a critical gap between aerial imaging and core sampling (see reviews by Scott *et al.*, 1990, Kneisel *et al.*, 2008, and Hauck, 2013). Their main strength has been to identify frozen vs. unfrozen ground, for example,

delineating the active layer and the base of permafrost. Electrical and electromagnetic methods have been widely applied because the quasi-static direct-current ('DC') resistivity of ice is very high compared to soils containing unfrozen water. Unfortunately, both dry materials and totally frozen ice-rich materials have high DC resistivity (e.g. Minsley *et al.*, 2012), so there is substantial ambiguity about the ice content. A recent approach to joint inversion of seismic and electrical data for rock, ice, water and air content (Hauck *et al.*, 2011) is useful for the near-uniform porosity and low clay content of rock glaciers, but is inappropriate for most permafrost soils due to variable porosity and additional clay conductivity.

There is, however, a unique property of frozen ground that heretofore has not been exploited in the field: its electrical polarisability. Whereas resistivity or conductivity measures energy dissipation through charge motion, electrical susceptibility or permittivity measures energy storage through the separation of bound charges. For example, ice polarisation in natural and synthetic permafrost samples has been

*Correspondence to: R. E. Grimm, Planetary Science Directorate, Southwest Research Institute, 1050 Walnut St #300, Boulder, Colorado 80302, USA. E-mail: grimm@boulder.swri.edu

characterised in the laboratory (Olhoeft, 1977; Bittelli *et al.*, 2004; Stillman *et al.*, 2010), and there is an even longer history of laboratory measurements of ice with soluble impurities (see Petrenko and Whitworth, 1999, for a review and Grimm *et al.*, 2008, and Stillman *et al.*, 2013a, 2013b, for newer findings). Yet in the field, the approach known as ‘induced polarisation’ has lagged the laboratory for permafrost, either lacking mention (Kneisel *et al.*, 2008; Hauck, 2013) or being identified as a significant challenge (Kemna *et al.*, 2012). The development of broadband, high-impedance field systems now enables geophysical measurements for ice content. In this paper, we first review the electrical properties of permafrost. We show how the classical frequency-domain resistivity frequency effect (RFE) is directly related to ice content as measured from laboratory data. We apply this technique to pilot field measurements in permafrost. Finally, we outline more advanced methods and suggest protocols for future surveys and long-term monitoring.

BACKGROUND

Materials respond to time-varying electric fields by a combination of dissipation and storage of energy and so can be represented by a single, frequency-dependent, complex number. Here, we focus on complex resistivity $\rho^* = \rho' + i\rho''$ ($i = \sqrt{-1}$), because the equivalent magnitude $|\rho| = \sqrt{\rho'^2 + \rho''^2}$ and phase $\phi = \text{atan}(\rho''/\rho')$ format are common in geophysics. Other formulations are possible in complex conductivity ($\sigma^* = 1/\rho^*$) and permittivity ($\epsilon^* = -i/\omega\rho^*$, where ω is the angular frequency). The real resistivity ρ' controls energy dissipation and the imaginary resistivity ρ'' determines the energy storage, so ϕ varies from zero for pure dissipation to -90° for pure storage.

Polarisability arises from specific charges, mobilities and length scales, often following a frequency-dependent behaviour called a dielectric relaxation. At low frequency (LF), bound charges can be fully separated over one cycle, manifesting the full polarisation. At high frequency (HF), the relevant charges cannot keep up with the applied field and are essentially unpolarisable. At some intermediate frequency – the relaxation frequency – charges move over nearly their full allowed extent over the course of the applied cycle. One useful description of a dielectric relaxation is the Cole-Cole formula (Cole and Cole, 1941), expressed here as complex conductivity:

$$\sigma^* = \sigma_S + \frac{\sigma_S m (i\omega\tau)^{1-\alpha}}{1 + (1-m)(i\omega\tau)^{1-\alpha}} + i\omega\epsilon_0\epsilon_\infty \quad (1)$$

where σ_S is the static or ‘DC’ conductivity, m is the chargeability, τ is the relaxation time constant, α is a parameter (0 for a classic Debye relaxation) that describes the distribution of relaxation length scales, ϵ_0 is the permittivity of free space and ϵ_∞ is the permittivity at

infinite frequency. This equation represents three circuit elements in parallel, and hence is easier to express in conductivity than resistivity. From left to right, these elements are a resistor that controls LF, a frequency-dependent impedance controlling the relaxation and a capacitor that controls HF. In real materials, multiple polarisation mechanisms can exist, so the second term is repeated with distinct properties for each relaxation. The last term is commonly omitted in geophysics where maximum frequencies are small compared to those studied here, but it is essential for measuring time constants correctly and for agreement with other fields such as material science (see Olhoeft, 1985; Jones, 1997).

The polarisability or energy storage in ice is due to protonic point defects: lattice sites where hydrogen atoms are improperly configured with respect to adjacent H₂O molecules (e.g. Petrenko and Whitworth, 1999). These charge defects (specifically, Bjerrum L-defects) can be rotated and have a characteristic dielectric relaxation. For ‘pure’ ice, in which all protonic point defects are intrinsic, the relaxation is close to Debye form and the relaxation frequency ($f_r = 1/2\pi\tau$) increases from 4 to 11 kHz as the temperature is increased from -10°C to 0°C . The corresponding minimum phase lag moves from 26 to 71 kHz. With the resistivity phase conventionally plotted, this minimum phase lag looks like a peak and we sometimes refer to it as such by analogy with spectra in other disciplines. Soluble impurities create additional, extrinsic defects, which increase the relaxation frequency. Variations in the electrical properties of natural and artificial ice samples have been extensively documented in laboratory studies (Petrenko and Whitworth, 1999, and references therein; Grimm *et al.*, 2008; Stillman *et al.*, 2013a, 2013b).

Silicates mixed with ice introduce additional polarisations (Olhoeft, 1976; Bittelli *et al.*, 2004; Stillman *et al.*, 2010; Grimm and Stillman, 2013) due to the interfacial, quasi-liquid water (~ 3 monolayers) and soluble ions present between ice and silicate (e.g. Anderson *et al.*, 1973; Sizemore *et al.*, 2014). We have identified a very HF relaxation due to H₂O rotation within the interfacial layer (analogous to the rotation of free water at even higher frequency), an intermediate-frequency signal of charge movement across the layer and an LF dispersion due to charge movement along the layer. The first and last are most evident at low saturation, low temperature and high silicate-specific surface area, but the intermediate relaxation of transverse charge motion can be important in fully saturated mixtures at higher temperatures.

Overall, the dielectric relaxations in ice-silicate mixtures are very strong, and therefore introduce very large differences in resistivity across the spectra. This is also manifested (by the Kramers-Kronig relations; e.g. Sihvola, 1999) as very large phase changes of tens of degrees. Furthermore, the relaxations are evident only because σ_s is small and does not ‘short-circuit’ the entire spectrum. This is quite distinct from induced polarisation at temperatures above freezing (e.g. Olhoeft, 1985; Breede and Kemna,

2012), in which net phases only of the order of 10 mrad ($<1^\circ$) are evident from water-mineral polarisations. This difference is one of several aspects of the electrical behaviour of frozen materials that enable robust laboratory and field characterisation.

LABORATORY MEASUREMENTS AND ANALYSIS

We measured the frequency- and temperature-dependent complex resistivity of samples of the Fairbanks silt acquired from within the US Army Cold Regions Research and Engineering Laboratory (CRREL) Permafrost Tunnel near Fox, Alaska (Sellman, 1967, 1972). We selected this location for an initial attempt at *in-situ* ice detection and characterisation using broadband complex resistivity because the site was well characterised in the literature (e.g. Arcone, 1984; Bjella *et al.*, 2008) and by previous DC resistivity surveys (Dinwiddie *et al.*, 2009). Also, the ice content in and around the tunnel was known to be very high. The Permafrost Tunnel comprises a horizontal adit and a smaller winze that slopes down and away from the adit. Using a Pomeroy drill, Dinwiddie *et al.* (2009) acquired seven core samples of the Fairbanks silt along the winze, distributed over both walls and the ceiling. Ice content, determined by melting and drying, varied from 44 to 100 per cent of the total sample volume (v%).

The 2.5 cm diameter cores were accommodated into the 3 cm diameter by 0.6 cm thick sample holder by partial melting and refreezing. Close fitting to a prescribed geometry allows more accurate recovery of absolute resistivity than estimating geometrical factors from an unconfined and surficially rough sample. We did not observe any significant change in the shapes of the amplitude and phase curves between as received and accommodated samples. There is little sensitivity to changes in geometry because the frequency-dependent dielectric properties of permafrost are dominated by volumetric effects, specifically the amount of ice and interfacial water.

Laboratory procedures are described by Grimm *et al.* (2008) and Stillman *et al.* (2010). Measurements were performed with a Solartron 1260A Impedance Analyzer with a 1296A Dielectric Interface front end. A ring-shaped PTFE sample holder is capped with two brass electrodes, plus a guard ring. This system is capable of measuring resistivities up to 10^{12} Ω -m and phases >0.1 mrad, with accuracies of 10 per cent and 5 per cent in the real and imaginary impedances, respectively. The impedance is converted to complex resistivity using the electrode geometry. Two-electrode measurements can be sensitive to electrode polarisation, which we identified as an LF 'asymptote' to about -5° phase instead of the expected zero value. However, this occurred only in the premelting regime approaching 0°C where the amount of unfrozen water dramatically increases. The resistivity is still very nearly flat with frequency here, so electrode polarisation does not significantly affect the results. In general, the

broadband measurement capability allows electrode polarisation to be readily identified as just another relaxation, and modelled out if necessary.

Measurements are swept from high to LF: the upper limit is always 1 MHz, but we rarely approach the lower limit of 1 mHz due to measurement time. Here, we report measurements down to 10 Hz. We commonly cool samples to -90°C and collect data while warming. This large temperature variation allows overlapping polarisation mechanisms to be identified by their chargeabilities and activation energies of their relaxation frequencies. Furthermore, measurements are more reproducible during warming without the possible confounding effects of metastable water.

The resistivity amplitude and phase spectra are dominated by DC conduction at LF, interfacial water relaxation at intermediate frequencies and ice relaxation at HF (Figure 1). These features were all identified in previous measurements of synthetic ice-silicate mixtures (Stillman *et al.*, 2010), and Cole-Cole modelling readily separates the individual contributions. It is significant that the interfacial water contribution to the broadband change in resistivity in this sample (Fairbanks silt 72 v% ice at -3°C) is approximately equal to that due to ice, whereas the interfacial water itself is ~ 2 v% (computed from Anderson *et al.*, 1973, and Sizemore *et al.*, 2014). This illustrates the large relative influence of the interfacial water, but as it is <3 per cent of the total H_2O volume, we will continue to label all H_2O as ice for the purposes of this paper.

The temperature dependencies of the relaxations (Figure 2) follow well-defined Arrhenius activation energies, which is a key property in identifying and exploiting them. The ice relaxation frequencies in the Fairbanks silt

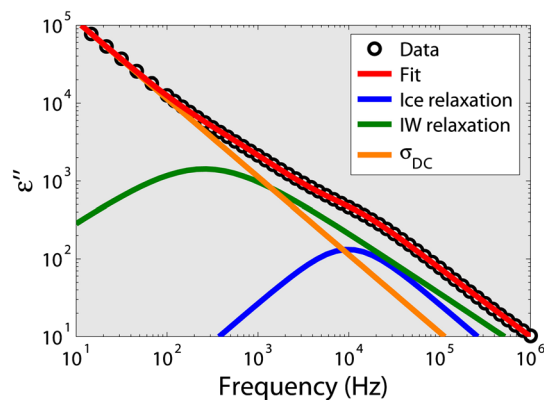


Figure 1 Imaginary component of relative dielectric permittivity ϵ'' of the Fairbanks silt (72 v% ice in this sample), measured in the laboratory at -3°C . Jointly fitting the real and imaginary parts to multiple Cole-Cole functions separates direct-current (DC) conductivity and the individual polarisabilities of ice and interfacial water (IW). These polarisabilities are approximately equal at 19 kHz in this sample. The quantity $\epsilon'' = \sigma'/\epsilon_0\omega$ (where σ' is the real conductivity, ϵ_0 is the permittivity of free space and ω is the angular frequency) is shown here because it peaks at the relaxation frequencies, highlighting the analogy of these process to traditional spectroscopy. This figure is available in colour online at wileyonlinelibrary.com/journal/ppp

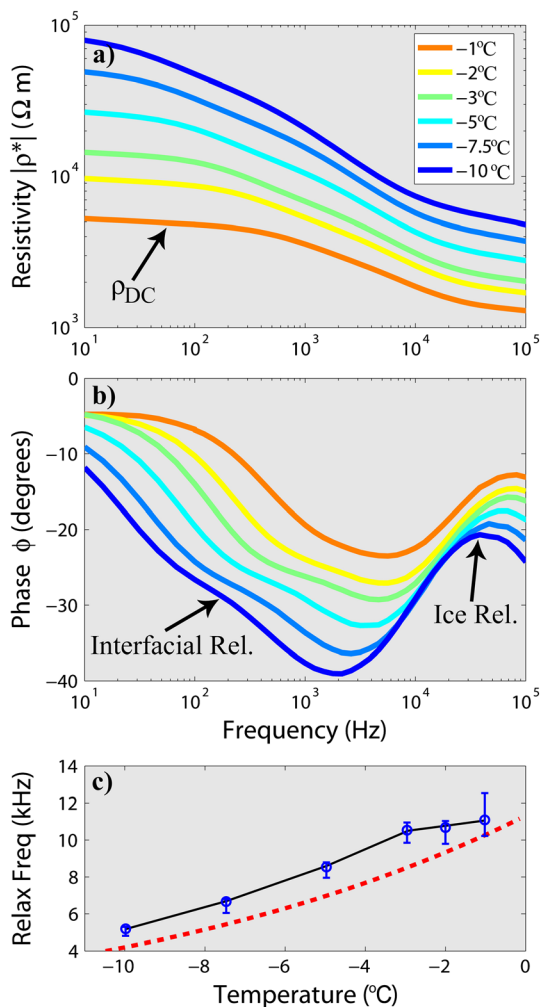


Figure 2 Variation in electrical properties of the Fairbanks silt (72 v% ice) as a function of temperature. (a) Resistivity magnitude. (b) Phase. Note temperature dependence of the phase 'peak' which is 2π higher in frequency than the formal relaxation. (c) Variation in ice relaxation frequency with temperature. Relaxation frequencies in ice are close to those of 'pure' ice (dashed line), indicating low-soluble impurity content. This figure is available in colour online at wileyonlinelibrary.com/journal/ppp

(Figure 2c) are close to those of pure H₂O (Auty and Cole, 1952). This is consistent with ice formation by slow freezing from a liquid in which soluble impurities are efficiently excluded (Grimm *et al.*, 2008). Chloride, the principal ice-soluble impurity, substitutes for oxygen but engenders extrinsic protonic defects due to its different charge. In contrast, polar meteoric ice, which nucleates in the atmosphere, incorporates up to 50 per cent of soluble impurities in the lattice (Stillman *et al.*, 2013a): this causes much faster dielectric relaxation.

Complex resistivity spectra change regularly with ice content (Figure 3). Using such data, the optimal approach to field (SIP) assessment of permafrost would be to extract the individual contributions of DC conductivity and the interfacial water and ice polarisations from laboratory

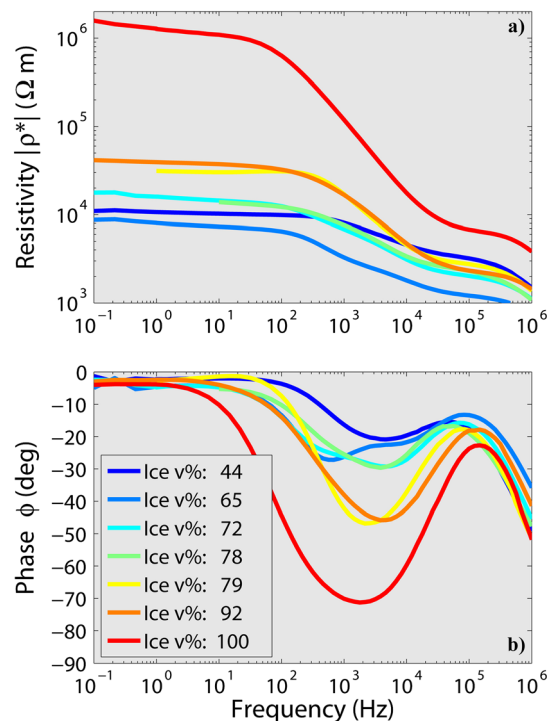


Figure 3 Variation in electrical properties of the Fairbanks silt as a function of the ice v% at -3°C . (a) Resistivity magnitude. (b) Phase. Note increasing contrast in both amplitude and phase with increasing ice content. This figure is available in colour online at wileyonlinelibrary.com/journal/ppp

measurements as functions of the H₂O fraction and temperature, and then develop mixing models to invert field spectra for these components. Although Cole-Cole fitting has been performed on spectra obtained in laboratory tanks (Kemna *et al.*, 2000) and in the field (Fiandaca *et al.*, 2012; Flores Orozco *et al.*, 2013), fitting multiple relaxations for the quantitative separation of different ground components has not yet been done. We outline such an approach in the Discussion. For this initial test, we sought a simple parameterisation of the spectrum that captured the essential H₂O signature: the large change in resistivity between 'low' and 'high' frequencies. The normalised difference between these quantities is defined as the RFE, ξ . The RFE approximates chargeability but it is not formally asymptotic and it includes chargeabilities of both ice and interfacial water. From the parameters of the field system (see below), we selected the resistivities at 10 Hz and 19.3 kHz as representative of the static- and infinite-frequency endmembers, so

$$\xi = \frac{\rho'_{10\text{Hz}} - \rho'_{19\text{kHz}}}{\rho'_{10\text{Hz}}} \quad (2)$$

At a fixed temperature, ξ of the Fairbanks silt (Figure 4) varies monotonically with ice volume fraction θ (apart from small experimental errors). We fit a simple power law to the laboratory data of $\theta(\xi) = a\xi^b + c$ at each measurement

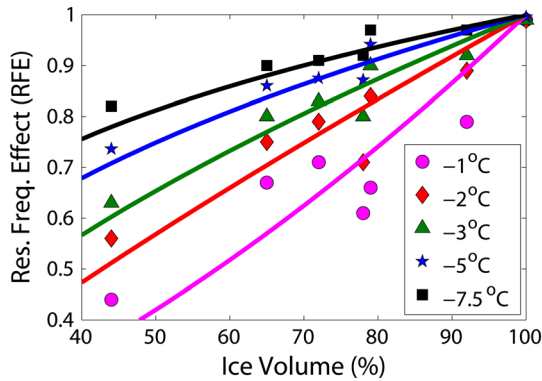


Figure 4 Laboratory measurements (symbols) of the resistivity frequency effect (RFE), $\xi = (\rho'_{10\text{Hz}} - \rho'_{19\text{kHz}}) / \rho'_{10\text{Hz}}$, where $\rho'_{10\text{Hz}}$ and $\rho'_{19\text{kHz}}$ are the real resistivities at 10 Hz and 19.3 kHz, respectively. Power law fits (lines) are used to invert ice volume from the RFE at each temperature. This figure is available in colour online at wileyonlinelibrary.com/journal/ppp

temperature (e.g. $a, b, c = 95.2, 1.75, 4.78$, respectively, at -3°C). The overall standard deviation on predicting ice content from the RFE is 6 per cent at a fixed temperature, but a 1°C difference in temperature translates up to ± 10 per cent in ice content. This can influence the accuracy of ice volume estimation.

FIELD METHODS

In the field, broadband frequency-domain complex resistivity measurements are known as SIP. SIP field surveys are geometrically identical to classical DC resistivity. The measured voltage and its phase between any pair of transmit and receive dipoles yield a spectrum of apparent resistivity and phase as functions of electrode position and offset, which are then inverted to recover true resistivity and phase as functions of surface position and depth.

We used the SIP Fuchs III by Radić Engineering of Berlin, Germany. This system has a 20 kHz bandwidth, high input impedance (100 M Ω), sends and receives digital signals to the transmitter and multiple receiver dipoles by fibre optic cable, and incorporates a remote reference dipole for noise reduction. The Fuchs system enables field measurements in cold regions because: (1) the high input impedance allows signals to be measured in spite of high contact resistance with frozen ground (here, ~ 200 k Ω); (2) the large bandwidth is sensitive to enough of the decrease in resistivity in frequency and change in phase to characterise the strength of the ice dielectric relaxation, and hence ice content; and (3) resistive ground and optical isolation allow electrode spreads of several tens of metres long without inductive coupling, even at HF. This in turn means that investigation depths of the order of tens of metres can be achieved. Stainless steel stakes were used for both transmitter and receiver dipoles: as in the laboratory, we observed

no significant electrode polarisation in frozen materials. We configured the Fuchs system to measure 24 log-spaced complex resistivities between 10 Hz and 19.3 kHz.

We performed an SIP survey on the adit side of the winze, on a line positioned from 2 to 18 m from the adit-winze intersection (Figure 5). The electrodes were emplaced into the winze wall and so the plane of the two-dimensional (2D) survey is horizontal, in the plane of Figure 5. The survey used dipole lengths a of 1 and 2 m and offsets $n = 1-6$ as space allowed. We also did a cross-tunnel test and a survey on the surface above the tunnel: although the apparent resistivity spectra confirm those of the principal survey, fewer measurements and a lower signal-to-noise ratio (SNR) did not produce satisfactory inversions.

We surveyed in both forward and reciprocal configurations. Many spectra had a positive phase at LF, sometimes non-reciprocally, which we attribute to inductive coupling with abundant metal artefacts in the tunnel as this was most evident when either the transmitter or receiver electrode was next to an artefact. We discarded spectra with (positive) phase $> 10^\circ$. Of an original 187 measurements, this left 62 transmitter-receiver configurations for inversion, 40 of which are independent (non-reciprocal). Because many cycles are transmitted at each frequency, the Fuchs software directly produces error estimates on the transfer impedances. Appendix 1 tabulates all of the final transfer resistances and their error estimates for each transmitter-receiver setup, at 10 Hz and 19.3 kHz.

We tested several approaches to inversion, all using RES2DINV (Loke and Barker, 1996; Geotomo Software: <http://www.geotomosoft.com>). First, the real part of the resistivity at 10 Hz and 19 kHz was separately inverted and compared to form an RFE image. This was not entirely satisfactory because it did not exploit the physical link between frequencies. Other workers (e.g. Kemna *et al.*, 2000; Flores Orozco *et al.*, 2013) have nonetheless produced useful multifrequency images this way, so we attribute the failure to the limited density of our data-set. We did not find the induced-polarisation (IP) procedures in RES2DINV, which

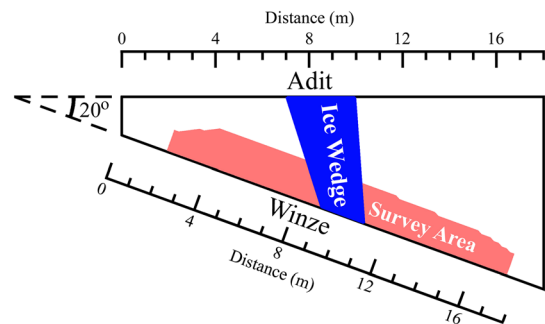


Figure 5 Horizontal projection of the adit-winze intersection in the Fox Permafrost Tunnel (Sellman, 1972), with position of the ice wedge taken from Arcone (1984). The spectral-induced polarisation survey was performed along the winze wall using 17 electrodes at locations 2–18 m; the interior area imaged after post-inversion editing is lightly shaded. This figure is available in colour online at wileyonlinelibrary.com/journal/ppp

use DC resistivity and chargeability, to be effective either, perhaps for the same reason.

We discovered a third approach that was quite successful: using the time-lapse feature of RES2DINV, we inverted the entire spectrum of real resistivity and derived the RFE from the results at 10 Hz and 19.3 kHz. The time-lapse algorithm assumes that each measurement is derived from the previous one and so applies a regularisation across successive measurements (Kim *et al.*, 2009). By treating the lowest frequency as ‘zero time’ and each successive frequency in the spectrum as a ‘time step’, smooth inversions could be obtained. Spatio-spectral regularisation was also implemented recently by Kemna *et al.* (2014). We assigned equal weight to reducing the differences between the models (images) at different frequencies and reducing the individual model roughness. Note that we did not fit phase explicitly, but this can be checked a posteriori using the Kramers-Kronig relations.

RESULTS

Representative apparent resistivity and phase data from the Permafrost Tunnel SIP survey (Figure 6) closely resemble laboratory measurements (Figures 1–3). Reciprocals of the winze survey were typically in good agreement. Spectra with minor inductive coupling were still useable. The resulting images of real resistivity at the two frequencies (Figure 7a, b) were cut off where the resistivity error (Figure 7e, f) estimated by RES2DINV exceeded 20 per cent (which occurred only for the HF image). This error estimate includes the misfit in reciprocals as well as specified data error. The resistivities are converted to RFE (Figure 7c; Equation 2) including error propagation (Figure 7g; Bevington, 1969). The root-mean-square (RMS) misfit between predicted and observed apparent resistivities is ~1.7 per cent at both endmember frequencies.

The conversion of the RFE to ice volume requires the choice of a temperature. We calculated the χ^2 misfit between the logarithm of the mean-inverted resistivity spectrum and the logarithm of the laboratory resistivity spectrum (Figure 8). The former is the average over all image pixels but includes all of the intermediate frequencies between 10 Hz and 19.3 kHz. The latter comprises the measurements for 44, 65, 72, 79, 92 and 100 per cent ice at temperatures of -1, -2, -3, -5 and -7.5 °C. The best fit was 79 per cent ice at -3 °C. A standard error $\sigma_T = 0.25$ °C follows the classical relationship (Bevington, 1969) $\sigma_T^2 = 2/(\partial^2\chi^2/\partial T^2)$, using a standard error 0.3 log units from the maximum in the resistivity data and assuming uncorrelated data errors. This formal error is smaller than our temperature sampling, so we adopt ± 0.5 °C as the temperature error from this exercise. The map of ice volume (Figure 7d) from the RFE at -3 °C has a mean of 81 per cent, in good agreement with the laboratory reference. The standard deviation on ice volume is 10 per cent. The estimated errors in ice volume (Figure 7h) propagate all previous errors, as well

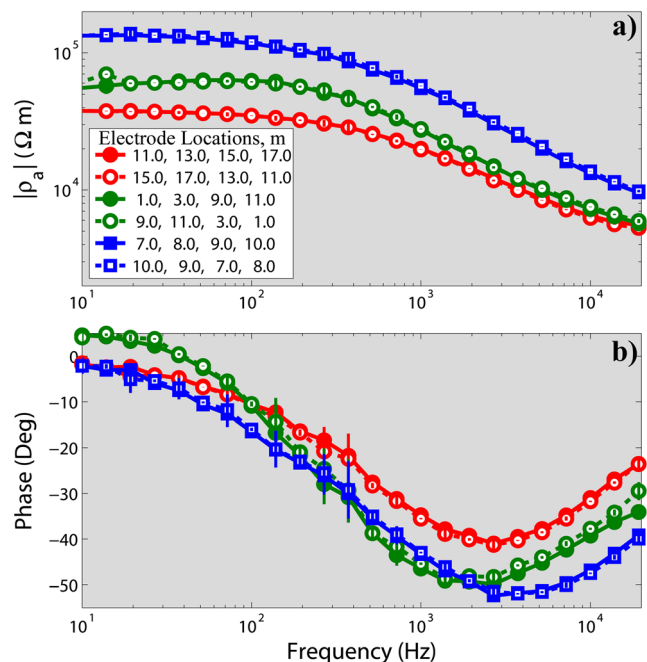


Figure 6 Examples of spectral-induced polarisation field data taken in the Fox Permafrost Tunnel. (a) apparent resistivity (b) phase. Forward measurements are solid symbols and reciprocals are open symbols. Error estimates, produced directly from the survey equipment, are generally smaller than the symbols, except near 60-Hz powerline noise and its harmonics. Red: $a = 2$, $n = 1$, near the end of the survey line. Green: $a = 2$, $n = 3$, with one dipole across the ice wedge. Blue: $a = 1$, $n = 1$, entering the ice wedge. Overall, the field spectra strongly resemble the laboratory measurements, showing large phases and changes in resistivity characteristic of the summed ice and interfacial water relaxations. Minor inductive coupling is evident in the long offset data (green) as a low-frequency positive phase and slope reversal in resistivity. This figure is available in colour online at wileyonlinelibrary.com/journal/ppp

as including a 6 per cent error on ice content due to temperature uncertainty.

The main feature of Figure 7d is a zone of very high ice content that slants from the surface through the full 2 m maximum depth of the image. This correlates very well with the position of an ice wedge, whose trace is inferred from exposures in both the winze and adit (Arcone, 1984). A zone of low ice content appears just before the ice wedge; this correlates with a region of prominent laminations and organic inclusions in the Fairbanks silt (Kanevskiy *et al.*, 2008).

The seven core samples in the winze (Dinwiddie *et al.*, 2009) had an ice volume of 76 ± 18 per cent. This agreement is reasonable overall with the SIP inversion: equality of the medians can only be rejected at $p = 0.37$ using the Wilcoxon rank-sum test (with Figure 7d downsampled to the number of original, independent data). However, the samples were not necessarily random, being chosen for variety. Note that point-by-point comparisons between the samples and the images are not useful: permafrost stratigraphy and structure in the tunnel can vary strongly on a submetre scale (see map of winze wall by Kanevskiy

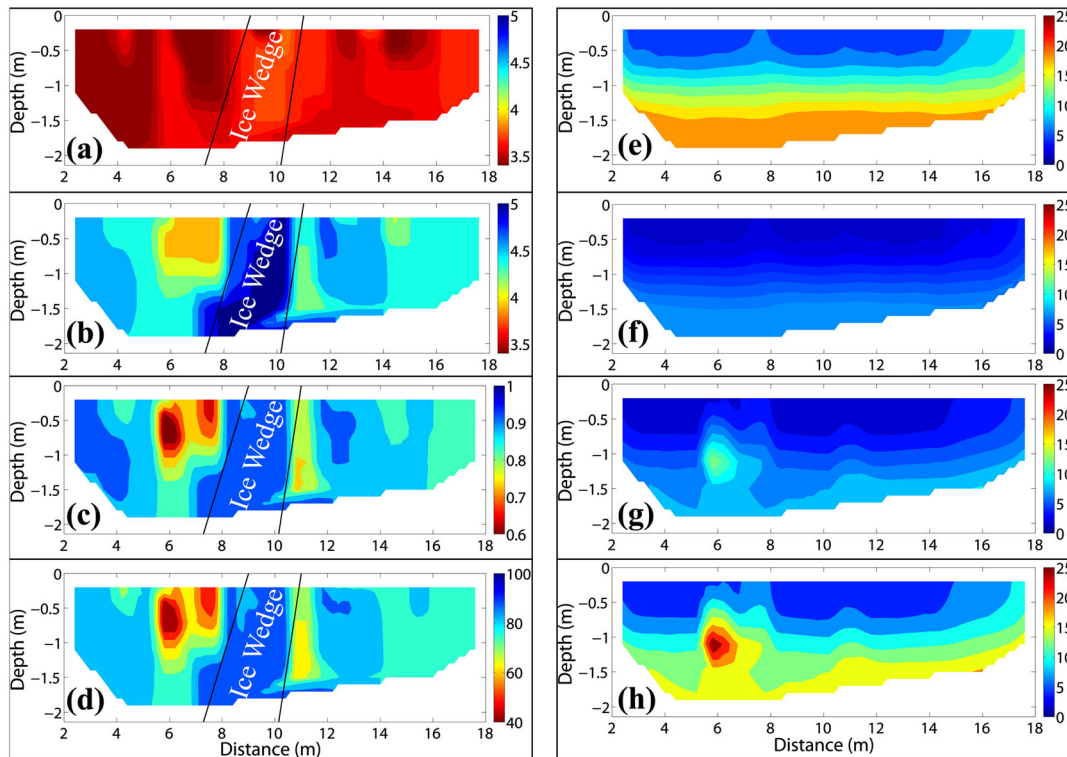


Figure 7 Spectral-induced polarisation horizontal section (two-dimensional survey/interpretation) in the north wall of the Fox Permafrost Tunnel winze. Coordinates and position of the ice wedge follow Figure 5. (a) High-frequency (HF) resistivity (19 kHz); (b) low-frequency (LF) resistivity (10 Hz); (c) resistivity frequency effect (RFE); (d) ice content, derived using laboratory measurements at -3°C ; (e–h) standard errors (in per cent) on columns a–d, respectively. The net error in ice content includes errors in HF and LF resistivities, the ice-RFE relation and temperature. This figure is available in colour online at wileyonlinelibrary.com/journal/ppp

et al., 2008), breaking any specific ties between the 3" diameter cores and the metre-scale image resolution. An average of several nearby cores might be appropriate to compare to the SIP field results, with groups of cores selected in distinct but nearly homogeneous zones. Consider that Sellman (1967) reported ice content in 45 samples from the adit, including four locations with multiple (5–9) closely spaced samples. Variations up to 20 per cent exist within these dense sampling locales, with standard deviations of 3–6 per cent. After averaging these locales, the reweighted ice content for Sellman's adit samples is 67 ± 7 per cent. Variability within sampling locales can therefore be comparable to that between locales. Also note that, after eliminating two of our samples taken from ice wedges (which Sellman avoided), ice contents of our winze samples are consistent with the same population as Sellman's adit samples (Wilcoxon rank sum $p = 0.43$). We conclude that the SIP-derived ice contents are consistent with the bulk composition of the permafrost tunnel and with large features; in the Discussion we return to point comparisons.

A wall temperature of $-3 \pm 0.5^{\circ}\text{C}$ inferred here is consistent with an air temperature of -3.4 to -3.1°C during our surveys (M. Cysewski, personal communication). In the past decade, air temperatures in the tunnel were between -3 and

-2°C , although there is evidence for excursions close to or exceeding 0°C at the rear of the adit (Bjella *et al.*, 2008). This poor environmental control is even more evident when comparing to temperatures measured three decades ago in wall cores (-4.6 to -7°C ; Arcone, 1984).

DISCUSSION

This study used a new generation of commercial equipment in a novel application, and so additional discussion of both possible limitations and future improvements is warranted.

Conventional SIP surveys are not carried out at the HF used here due to inductive coupling. The induction number B (electromagnetic skin depth/array length) is relatively small (< 0.05) in this study, due to the high resistivity in frozen ground ($\sim 4000 \Omega\text{-m}$ at 19.3 kHz) and relatively small array lengths ~ 10 m. Nonetheless, inductive phase errors up to a few degrees could be introduced (e.g. Figure 5 in Dey and Morrison, 1973). However, the phase changes of tens of degrees caused by the ice and interfacial water polarisations are much larger than those due to inductive coupling. The only serious problems that we had with inductive coupling were likely due to metal embedded in the tunnel wall.

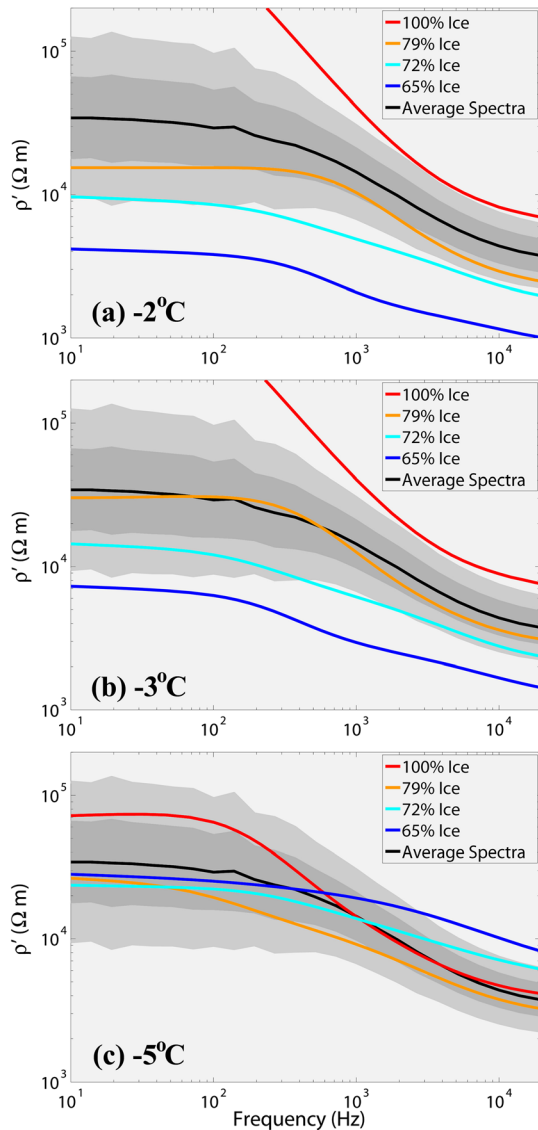


Figure 8 Comparison of laboratory data (colour) to an ensemble of inverted field data (black = mean; dark grey = 68th percentile; light grey = 95th percentile). Best fit of the mean spectrum to the laboratory data is the 79 v% sample at -3 °C. Ice content in the winze wall (Figure 7c) is then computed to be 81 ± 10 per cent. This figure is available in colour online at wileyonlinelibrary.com/journal/ppp

We also considered the effects of capacitive coupling: at HF or large dipole length, the reactance of the wires connecting the electrodes becomes lower than the electrode resistance, giving erroneous transmitter properties and receiver readings. However, we observed no systematic variation with frequency or dipole size either in these data or in subsequent follow-up surveys in frozen ground near Tok, Alaska (Stillman *et al.*, 2014). There SIP data were acquired with transmitter dipoles up to 12.5 m long, and 5 m dipoles were compared directly to Geometrics OhmMapper data. The latter is a capacitively coupled resistivity (CCR) system (by design) operating at 16.5 kHz.

The particular geometry of the Permafrost Tunnel, with finite cross-sections of the adit and winze and their proximity, suggests that three-dimensional (3D) effects might be important: currents will flow out of the horizontal plane and around the tunnels, and the adit might be sensed from the winze. We tested a 2D forward model in a vertical plane perpendicular to the tunnels, and found that the difference in voltage with a uniform halfspace in the survey plane was <10 per cent. Geoelectrical measurements are most sensitive to the region directly below the electrodes (e.g. Loke, 2014), so to obtain a significant 3D effect a survey must be designed for it (e.g. cross-tunnel).

Future studies can exploit both resistivity amplitude and phase across the full spectrum. Here, we showed a spectrally regularised inversion of amplitude data, and inversions for complex resistivity are now becoming the norm. Our main contribution heretofore has been separation and identification in the laboratory of the individual electrical conduction and polarisation mechanisms: the same approach can be applied to field data. We then require constitutive relations or mixing models that relate model parameters to volumes of silicate, ice and interfacial water. Generalisation is an important outstanding issue: can constitutive relations be transferred to other sites? We chose the Fox Permafrost Tunnel for initial tests because of known high ice content and prior geophysical characterisation, but a site incorporating a full range from zero to near 100 per cent ice would provide robust validation.

An important part of the workflow was determining the ground temperature from the spectra, as this is required for selection of the correct curve relating the RFE to ice content. Our stated accuracy for this simple approach is ± 0.5 °C: because the formal error was smaller, we took half of the temperature measurement increment as an upper limit. A denser spacing of laboratory measurements in both ice fraction and temperature would tighten these constraints. However, in a generalised constitutive relation derived from such measurements, the chargeabilities of ice and interfacial water will be specified as functions of both parameters. Furthermore, the measured activation energies of the relaxation frequencies may give a direct indicator of temperature. If these new approaches to the data analysis are combined with higher SNR from both spatially denser setups and reduced cultural noise, temperature errors may be reduced to ~ 0.1 °C. With such accuracy, spatial variations in temperature can be mapped without drilling (e.g. geothermal gradients or top-down propagation of long-term surface temperature variations).

Productivity is another issue, as SIP is very slow to acquire compared to automatically switched, multielectrode DC resistivity or mobile CCR. Stillman *et al.* (2014) describe a comparison of DC, SIP and CCR that suggests the RFE between the DC and CCR may be used to measure ice content. Spot soundings with SIP will likely still be necessary for calibration.

The techniques demonstrated here will have value for permafrost studies, infrastructure assessment and perhaps extraterrestrial exploration (Grimm and Stillman, 2011; Grimm *et al.*, 2014).

CONCLUSION

We measured the complex resistivity of natural permafrost samples from 10Hz to 19.3 kHz. We found that the spectra were dominated by DC resistivity and dielectric relaxations in ice and in the interfacial, liquid-like layer between ice and silicates. The RFE, approximating total chargeability, increases with ice content but is temperature dependent. Simple functions could then be fit to the laboratory data for ice content as a function of the RFE and temperature. We performed dipole-dipole SIP field surveys over the same frequency band and found that the field spectra were similar to laboratory measurements. The mean fractional ice volume derived from the field data using the laboratory RFE relations agreed reasonably with the mean measured from samples, but point comparisons were ineffective due to local sampling heterogeneity in the tunnel up to 20 per cent. The zone of highest ice content correlated well with a known ice wedge, and the zone of lowest ice content was associated with prominent laminations and organic inclusions in the host silt. The temperature in the wall inferred from SIP matched well the ambient air temperature -3 °C. Future improvements to the approach can include extraction of constituents by full fitting of the full amplitude and phase spectra. This will also enable more accurate temperature measurements of the subsurface.

ACKNOWLEDGEMENTS

We are grateful to Kevin Bjella and Margaret Cysewski (U.S. Army Cold Regions Research and Engineering Laboratory) for support at the Fox Permafrost Tunnel, and Ronald McGinnis and Cynthia Dinwiddie (Southwest Research Institute) for discussion of prior geophysical surveys there. We thank three anonymous reviewers for detailed and constructive comments. This work was funded by SwRI Internal Research grants R8374 and R8422.

APPENDIX: Fox Permafrost Tunnel Electrical Survey Data*

A (m)	B (m)	M (m)	N (m)	R(19 kHz) (Ω)	σ(19 kHz)	R(10Hz) (Ω)	σ(10Hz)
2	1	3	4	217.30	0.8%	1757.0	0.4%
3	2	4	5	174.70	0.8%	1605.0	1.0%
4	3	5	6	148.60	1.3%	478.5	0.1%
8	7	9	10	507.20	1.0%	7084.0	0.7%
9	8	10	11	174.90	1.1%	1653.0	1.3%
13	14	11	12	117.50	1.1%	856.8	0.2%

(Continues)

(Continued)

A (m)	B (m)	M (m)	N (m)	R(19 kHz) (Ω)	σ(19 kHz)	R(10Hz) (Ω)	σ(10Hz)
12	13	10	11	305.50	0.9%	3515.0	1.1%
10	11	8	9	203.60	2.6%	1767.0	3.6%
9	10	7	8	520.40	2.1%	7095.0	3.1%
2	1	4	5	46.35	0.8%	517.7	1.2%
4	3	6	7	42.63	2.3%	124.2	0.4%
6	5	8	9	29.70	1.2%	235.5	2.4%
13	14	10	11	47.55	1.0%	397.4	0.6%
2	1	5	6	15.31	0.7%	86.1	0.4%
3	2	6	7	14.32	0.8%	52.0	0.6%
4	3	7	8	27.41	3.1%	183.5	1.2%
5	4	8	9	25.91	0.2%	187.9	0.6%
6	5	9	10	28.37	5.3%	226.8	1.1%
9	10	5	6	34.09	2.0%	227.1	3.5%
8	9	4	5	19.10	0.7%	182.4	2.7%
7	8	3	4	24.68	3.6%	183.7	1.4%
2	1	6	7	7.84	0.7%	29.2	0.7%
3	2	7	8	11.35	1.7%	115.3	1.8%
4	3	8	9	8.38	1.7%	103.1	2.2%
9	10	4	5	21.37	2.0%	189.4	1.9%
8	9	3	4	8.40	0.7%	102.4	2.2%
2	1	7	8	6.52	0.8%	70.9	1.6%
3	2	8	9	4.01	0.8%	80.7	2.5%
4	3	9	10	11.38	1.9%	103.2	0.7%
9	10	3	4	11.08	1.6%	103.9	3.8%
8	9	2	3	5.20	0.8%	80.2	2.9%
7	8	1	2	6.73	3.1%	71.3	1.8%
2	1	8	9	2.40	0.8%	50.5	2.7%
3	2	9	10	5.88	2.4%	72.6	1.1%
9	10	2	3	7.02	3.3%	74.9	3.0%
8	9	1	2	2.87	0.7%	50.1	2.5%
1	3	5	7	72.75	1.0%	347.6	0.0%
2	4	6	8	79.71	1.5%	478.9	1.1%
3	5	7	9	130.70	1.5%	876.3	2.0%
4	6	8	10	121.70	1.9%	837.5	0.6%
5	7	3	1	79.33	1.6%	347.4	0.0%
6	8	4	2	89.70	1.3%	477.0	0.8%
7	9	5	3	116.60	1.3%	803.7	1.6%
8	10	6	4	104.60	1.2%	824.6	3.1%
9	11	13	15	97.41	1.5%	795.7	2.1%
11	13	15	17	147.10	0.9%	1004.0	0.5%
13	15	11	9	101.60	1.1%	817.4	0.5%
14	16	12	10	104.50	1.2%	897.9	1.4%
15	17	13	11	139.90	2.0%	1005.0	1.0%
1	3	6	8	40.57	1.2%	267.6	1.1%
2	4	7	9	40.45	1.6%	481.7	2.2%
3	5	8	10	61.04	2.4%	580.1	0.9%
6	8	3	1	41.69	1.9%	267.5	1.2%
7	9	4	2	49.68	1.8%	487.5	2.1%
8	10	5	3	55.69	1.1%	580.7	2.4%
9	11	14	16	57.77	1.6%	516.8	1.9%
14	16	11	9	66.93	1.2%	521.0	0.9%
15	17	12	10	50.78	3.0%	376.6	1.3%
1	3	7	9	23.19	1.3%	287.7	2.4%
2	4	8	10	24.45	2.1%	357.0	1.2%
1	3	9	11	15.10	1.9%	147.0	1.2%
9	11	3	1	15.73	3.5%	163.7	3.1%

* Includes reciprocals. AB, MN = Transmitter and receiver dipole positions; R = transfer resistance, respectively; σ = standard error.

REFERENCES

- Anderson DM, Tice AR, McKim HL. 1973. The unfrozen water and the apparent specific heat capacity of frozen soils. In *Permafrost: North American Contribution to the Second International Conference National Academy of Sciences*: Washington, 289–295.
- Arcone SA. 1984. Pulse transmission through frozen silt. U.S Army Cold Regions Research and Engineering Laboratory Technical Report 84–71, Hanover: New Hampshire.
- Auty RP, Cole RH. 1952. Dielectric Properties of Ice and Solid D₂O. *The Journal of Chemical Physics* **20**: 1309–1314. DOI: 10.1063/1.1700726
- Bevington PR. 1969. *Data Reduction and Error Analysis for the Physical Sciences*. McGraw Hill: New York, 336.
- Bittelli M, Flury M, Roth K. 2004. Use of dielectric spectroscopy to estimate ice content in frozen porous media. *Water Resources Research* **40**: W04212. DOI: 10.1029/2003WR002343
- Bjella K, Tantillo T, Weale J, Lever J. 2008. Evaluation of the CRREL Permafrost Tunnel. U.S. Army Cold Regions Research and Engineering Laboratory Technical Report Hanover: New Hampshire, 08–11.
- Breede K, Kemna A. 2012. Spectral induced polarization measurements on variably saturated sand-clay mixtures. *Near Surface Geophysics* **10**: DOI: 10.3997/1873-0604.2012048
- Cole KS, Cole RH. 1941. Dispersion and Absorption in Dielectrics I. Alternating Current Characteristics. *The Journal of Chemical Physics* **9**: 341–351. DOI: 10.1063/1.1750906
- Dey A, Morrison HF. 1973. Electromagnetic coupling in frequency and time-domain induced-polarization surveys over a multilayered earth. *Geophysics* **38**: 380–405. DOI: 10.1190/1.1440348
- Dinwiddie CL, McGinnis R, Stillman D, Grimm RE, Hooper DM, Bjella K. 2009. Integrated Geophysical Examination of the CRREL Permafrost Tunnel's Fairbanks Silt Units, Fox, Alaska. AGU Fall Meeting Abstracts-1: 0429.
- Fiandaca G, Auken E, Christiansen A, Gazoty A. 2012. Time-domain-induced polarization: Full-decay forward modeling and 1D laterally constrained inversion of Cole-Cole parameters. *Geophysics* **77**: E213–E225. DOI: 10.1190/geo2011-0217.1
- Flores Orozco A, Williams KH, Kemna A. 2013. Time-lapse spectral induced polarization imaging of stimulated uranium bioremediation. *Near Surface Geophysics* **11**: DOI: 10.3997/1873-0604.2013020
- French HM. 2007. *The Periglacial Environment*. Third Edition. John Wiley and Sons: Chichester.
- Grimm RE, Stillman DE. 2011. Progress in Prospecting for Near-Surface H₂O on the Moon and Mars with Dielectric Spectroscopy. In *Lunar and Planetary Science Conference*, Lunar and Planetary Science Conference, 2550.
- Grimm RE, Stillman DE. 2013. Complex conductivity laboratory measurements of ice-silicate mixtures. In *Cryosphere Geophysics: Understanding a Changing Climate with Subsurface Imaging*, SEG/AGU Joint Workshop, 6–8 January 2013, Boise State University, Boise, Idaho.
- Grimm RE, Stillman DE, Dec SF, Bullock MA. 2008. Low-Frequency Electrical Properties of Polycrystalline Saline Ice and Salt Hydrates. *The Journal of Physical Chemistry B* **112**: 15382–15390. DOI: 10.1021/jp8055366
- Grimm RE, Stillman DE, McGinnis RN. 2014. Characterization of ground ice using complex resistivity. *Geol. Soc. Amer. Ann. Mtg*, Paper 84-1.
- Hauck C. 2013. New Concepts in Geophysical Surveying and Data Interpretation for Permafrost Terrain. *Permafrost and Periglacial Processes* **24**: 131–137. DOI: 10.1002/ppp.1774
- Hauck C, Böttcher M, Maurer H. 2011. A new model for estimating subsurface ice content based on combined electrical and seismic data sets. *The Cryosphere* **5**: 453–468. DOI: 10.5194/tc-5-453-2011
- Heginbottom J, Brown J, Humlum O, Sennson H. 2012. Permafrost and periglacial environments, In *State of the Earth's Cryosphere at the Beginning of the 21st Century*, Williams R, Ferrigno J (eds). USGS Professional Paper 1386-A-5, 546.
- Jones D. 1997. Investigation of Clay-Organic Reactions Using Complex Resistivity, MS Thesis, Colorado School of Mines: Golden, Colorado, 378.
- Jorgenson MT, Osterkamp TE. 2005. Response of boreal ecosystems to varying modes of permafrost degradation. *Canadian Journal of Forest Research* **35**: 2100–2111. DOI: 10.1139/x05-153
- Kanevskiy M, Fordier D, Shur Y, Bray M, Jorgenson T. 2008. Detailed cryostratigraphic studies of syngenetic permafrost in the winze of the CRREL permafrost tunnel, Fox, Alaska. *Proceedings of the Ninth International Conference on Permafrost* **1**: 889–894.
- Kemna A, Binley A, Ramirez A, Daily W. 2000. Complex resistivity tomography for environmental applications. *Chemical Engineering Journal* **77**: 11–18. DOI: 10.1016/S1385-8947(99)00135-7
- Kemna A, Binley A, Cassiani G, Niederleithinger E, Revil A, Slater L, Williams KH, Orozco AF, Haegel F-H, Hördt A, Kruschwitz S, Leroux V, Titov K, Zimmermann E. 2012. An overview of the spectral induced polarization method for near-surface applications. *Near Surface Geophysics* **10**: DOI: 10.3997/1873-0604.2012048
- Kemna A, Huisman JA, Zimmermann E, Martin R, Zhao Y, Treichel A, Flores Orozco A, Fechner T. 2014. Broadband electrical impedance tomography for subsurface characterization using improved corrections of electromagnetic coupling and spectral regularization. In *Tomography of the Earth's Crust: From Geophysical Sounding to Real-Time Monitoring*, Weber M, Münch U (eds). *GEOTECHNOLOGIEN Science Report* 21:1–20.
- Kim J-H, Yi M-J, Park S-G, Kim J-G. 2009. 4-D inversion of DC resistivity monitoring data acquired over a dynamically changing earth model. *Journal of Applied Geophysics* **68**: 522–532. DOI: 10.1016/j.jappgeo.2009.03.002
- Kneisel C, Hauck C, Fortier R, Moorman B. 2008. Advances in geophysical methods for permafrost investigations. *Permafrost and Periglacial Processes* **19**: 157–178. DOI: 10.1002/ppp.616
- Loke MH. 2014. Tutorial: 2D and 3D Electrical Imaging Surveys. Geotomo Software: Penang, Malaysia.
- Loke MH, Barker RD. 1996. Rapid least-squares inversion of apparent resistivity pseudosections by a quasi-Newton method. *Geophysical Prospecting* **44**: 131–152. DOI: 10.1111/j.1365-2478.1996.tb00142.x
- Minsley BJ, Abraham JD, Smith BD, Cannia JC, Voss CI, Jorgenson MT, Walvoord MA, Wylie BK, Anderson L, Ball LB, Deszcz-Pan M, Wellman TP, Ager TA. 2012. Airborne electromagnetic imaging of discontinuous permafrost. *Geophysical Research Letters* **39**: L02503. DOI: 10.1029/2011GL005079
- Olhoeft GR. 1977. Electrical properties of natural clay permafrost. *Canadian Journal of Earth Sciences* **14**: 16–24. DOI: 10.1139/e77-002
- Olhoeft GR. 1985. Low-frequency electrical properties. *Geophysics* **50**: 2492–2503.
- Petrenko VF, Whitworth RW. 1999. *Physics of Ice*. Oxford University Press.
- Schuur EAG, Bockheim J, Canadell JG, Euskirchen E, Field CB, Goryachkin SV, Hagemann S, Kuhry P, Laflour PM, Lee H, Mazhitova G, Nelson FE, Rinke A, Romanovsk VE, Shiklomanov N, Tarnocai C, Venevsk S, Vogel JG, Zimov SA. 2008. Vulnerability of Permafrost Carbon to Climate Change: Implications for the Global Carbon Cycle. *BioScience* **58**: 701–714. DOI: 10.1641/B580807
- Scott WJ, Sellman PV, Hunter JA. 1990. Geophysics in the study of permafrost. In *Geotech. and Environ. Geophys.*, Vol 1,

- Ward SH (ed), *Invest. Geophys.*, 5. Soc. Explor. Geophys.: Tulsa; 355–384.
- Sellman PV. 1967. Geology of the USA CRREL Permafrost Tunnel, Fairbanks, Alaska. U.S Army Cold Regions Research and Engineering Laboratory Technical Report **199**: Hanover, New Hampshire.
- Sellman PV. 1972. Geology and Properties of Materials Exposed in the USA CRREL Permafrost Tunnel, U.S Army Cold Regions Research and Engineering Laboratory Special Report **177**.
- Sihvola AH. 1999. Electromagnetic Mixing Formulas and Applications, Institution of Electrical Engineers: Stevenage.
- Sizemore HG, Zent AP, Rempel AW. 2014. Initiation and growth of martian ice lenses. *Icarus*. DOI: 10.1016/j.icarus.2014.04.013
- Stillman DE, Grimm RE, Dec SF. 2010. Low-Frequency Electrical Properties of Ice–Silicate Mixtures. *The Journal of Physical Chemistry B* **114**: 6065–6073. DOI: 10.1021/jp9070778
- Stillman DE, MacGregor JA, Grimm RE. 2013a. Electrical response of ammonium-rich water ice. *Annals of Glaciology* **54**: 21–26. DOI: 10.3189/2013AoG64A204
- Stillman DE, MacGregor JA, Grimm RE. 2013b. The role of acids in electrical conduction through ice. *Journal of Geophysical Research: Earth Surface* **118**: 1–16. DOI: 10.1029/2012JF002603
- Stillman DE, Grimm RE, McGinnis RN. 2014. Subsurface ice detection via low-frequency surface electromagnetic methods. Amer. Geophys. Union, Fall Mtg, NS34A-03.